atmosphere

Article

Spatial-Temporal Variation of AOD Based on MAIAC AOD in East Asia from 2011 to 2020

Ping Wang [1], Qingxin Tang [1,*], Yuxin Zhu [2], Yaqian He [3], Quanzhou Yu [1], Tianquan Liang [1] and Ke Zheng [1]

1 College of Geography and Environment, Liaocheng University, Liaocheng 252059, China
2 School of Urban and Environmental Sciences, Huaiyin Normal University, Huaian 223300, China
3 Department of Geography, University of Central Arkansas, Conway, AR 72034, USA
* Correspondence: tangqingxin@lcu.edu.cn

Abstract: In recent years, atmospheric aerosol pollution has seriously affected the ecological environment and human health. Understanding the spatial and temporal variation of AOD is essential to revealing the impact of aerosols on the environment. Based on the MAIAC AOD 1 km product from 2011 to 2020, we analyzed AOD's distribution patterns and trends in different time series across East Asia. The results showed that: (1) The annual average AOD in East Asia varied between 0.203 and 0.246, with a decrease of 14.029%. The areas with high AOD values were mainly located in the North China Plain area, the Sichuan Basin area, and the Ganges Delta area, with 0.497, 0.514, and 0.527, respectively. Low AOD values were mainly found in the Tibetan Plateau and in mountainous areas north of 40° N, with 0.061 in the Tibetan Plateau area. (2) The distribution of AOD showed a logarithmic decreasing trend with increasing altitude. Meanwhile, the lower the altitude, the faster the rate of AOD changes with altitude. (3) The AOD of East Asia showed different variations in characteristics in different seasons. The maximum, minimum, and mean values of AOD in spring and summer were much higher than those in autumn and winter. The monthly average AOD reached a maximum of 0.326 in March and a minimum of 0.190 in November. The AOD showed a continuous downward trend from March to September. The highest quarterly AOD values in the North China Plain occurred in summer, while the highest quarterly AOD values in the Sichuan Basin, the Ganges Delta, and the Tibetan Plateau all occurred in spring, similar to the overall seasonal variation in East Asia.

Keywords: MAIAC AOD; East Asia; spatial-temporal pattern; trend analysis

check for updates

Citation: Wang, P.; Tang, Q.; Zhu, Y.; He, Y.; Yu, Q.; Liang, T.; Zheng, K. Spatial-Temporal Variation of AOD Based on MAIAC AOD in East Asia from 2011 to 2020. *Atmosphere* **2022**, *13*, 1983. https://doi.org/10.3390/atmos13121983

Academic Editors: Hongmin Zhou, Tao He, Xiaodan Wu and Ying Qu

Received: 2 November 2022
Accepted: 24 November 2022
Published: 27 November 2022

1. Introduction

Aerosols are small solid and liquid particles suspended in the air, with aerodynamic diameters ranging from 10^{-3} µm to 100 µm [1]. Aerosols have an important role in climate and environment at regional and global scales. They can not only affect atmospheric visibility [2] but also directly absorb and scatter solar radiation, which is an important parameter for maintaining the Earth–atmosphere radiation balance [3]. Aerosols can also directly affect cloud formation processes through aerosol–cloud interactions [4] and indirectly amplify or dimmish warming caused by climate change [5]. In addition, aerosols have important effects on human health [6,7]. Meanwhile, aerosols are highly variable in space and time [8]. The long-term trends and interannual variability of aerosols are critical for climate change and environmental quality assessment. Aerosol optical properties are the main factors affecting atmospheric radiation. As one of the aerosol optical parameters, Aerosol Optical Depth (AOD) can be used to represent regional aerosol loading [9] and reveal the effects of aerosol on radiation, and thereby global climate.

The methods to monitor AOD mainly include ground-based and satellite-based methods. Ground-based monitoring networks have been used across countries and regions worldwide. The observations they provided have improved the understanding of the spatial and temporal distribution of AOD and its impact on climate [10]. However, ground-based networks have limitations in both spatial and temporal coverage. Satellite remote sensing well avoids this drawback and provides systematic real-time AOD observation from low to high spatial resolution [11,12]. It is considered an effective method for long-term monitoring of AOD's spatiotemporal distribution. Based on Landsat 8 Operational Land Imager (OLI) images and MODIS09A1 surface reflectance products, Jin et al. [13] retrieved and analyzed AOD's distribution patterns in different seasons in Nanjing City from 2017 to 2018 using the combined Dark Target (DT) and Deep Blue (DB) methods. At a larger scale, Li et al. [14] analyzed the spatiotemporal distribution of aerosols and dust transportation in the Tibet Plateau and Tarim Basin using Modern Era Retrospective-Analysis for Research and Applications, Version 2 (MERRA-2) data, and Cloud-Aerosol Lidar and Infrared Pathfinder Satellite Observation (CALIPSO) data. In addition, to monitor the AOD over land, Wang et al. [15] analyzed the spatial patterns of the AOD and found a significant north–south difference with a boundary of 25° N using the field observation data and AVHRR remote sensing data over the Western Pacific Ocean.

The Moderate Resolution Imaging Spectroradiometer (MODIS) on the Terra and Aqua satellites provides daily global aerosol data [16]. As one of the most commonly used satellite sensors, MODIS provides available terrestrial aerosol products based on the DT [17] and DB algorithms [18]. The AOD products performed well regionally and globally [19] and have been used in relevant studies worldwide. Cheng et al. [20] produced a dataset to unravel the spatiotemporal characteristics of aerosols over the Pan Yangtze River Delta region from 2014 to 2017 by merging the MODIS 3 km resolution DT AOD with the 10 km resolution DB AOD data by linear regression. Similarly, Shen et al. [21] analyzed spatiotemporal variations of aerosol optical properties over the Yellow and Bohai Seas from 2002 to 2017 using MODIS DT AOD observations at 550 nm. Boiyo et al. [22] compared and analyzed the long-term (2002–2016) spatiotemporal distribution and trends of AOD over East Africa retrieved from the MODIS Aqua (DT and DB) and multi-angle imaging spectroradiometer (MISR). Besides MODIS DT and DB AOD products, the MCD19A2, a Multi-Angle Implementation of Atmospheric Correction (MAIAC) terrestrial AOD gridded level 2 product, also shows high spatial coverage, retrieval frequency, and accuracy. The MCD19A2, with a spatial resolution of 1 km, combines MODIS Terra and Aqua [23]. It has the ability to distinguish aerosol sources and identify fine aerosol features [24]. Soleimany et al. [25] verified the MCD19A2 AOD product and proved that MCD19A2 could accurately indicate the aerosol distribution in the Khuzestan province of Iran. In a recent study, Dong et al. [26] identified the temporal and spatial distribution of AOD, Ångström wavelength index (AE), and aerosol types in the Beijing–Tianjin–Hebei region based on the ecological functional zones from 2015 to 2020, using MCD19A2 and MOD04_3K products.

East Asia is one of the major source regions of dust aerosols on Earth, producing a large number of dust particles each year [27]. The growing economies, dense populations, and industrialization have led to increased aerosols and affected air quality, agriculture, and water resources in East Asia [28,29]. East Asia has become an aerosol hot spot where natural and anthropogenic aerosols co-exist [30,31]. The patterns of AOD are in a state of flux and remain unknown due to spatiotemporal variations. Understanding the spatial and temporal variability of AOD in East Asia is important for atmospheric environmental and life health protection.

This study aims to thoroughly assess the spatiotemporal variations of AOD in East Asia from 2011 to 2020. We used the MCD19A2 AOD data with 1 km spatial resolution to examine the annual, seasonal, and monthly variations and trends of AOD in East Asia.

2. Data and Methods

This study area includes eastern and central China, Mongolia, the Democratic People's Republic of Korea, the Republic of Korea, Laos, Cambodia, the Philippines, Thailand, and Vietnam, and some regions in Myanmar, Japan, and Malaysia, as shown in Figure 1.

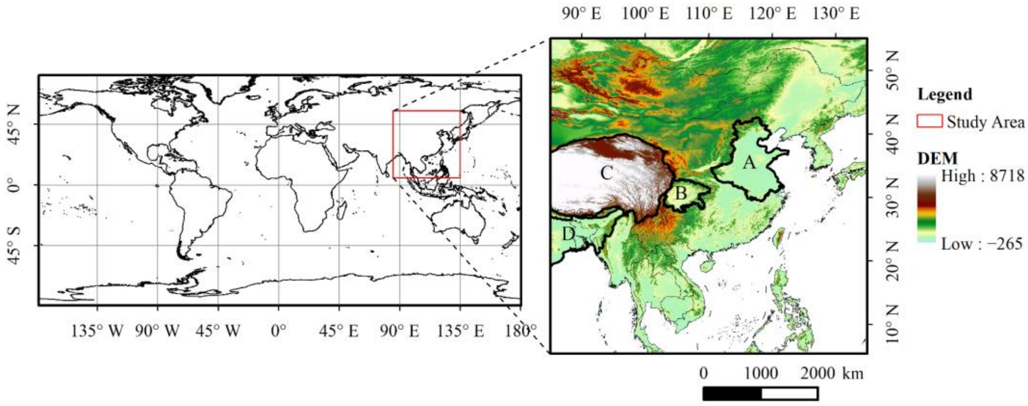

Figure 1. Study area A: the North China Plain area, B: the Sichuan Basin area, C: the Qinghai-Tibet Plateau area, D: the Ganges Delta area.

2.1. Data

2.1.1. MAIAC AOD

In this study, we used the MCD19A2 (2011–2020) dataset at 550 nm. MCD19A2 Collection 6 (MAIAC aerosol product) was obtained from the National Aeronautics and Space Administration (NASA) Goddard Space Flight Center (https://earthdata.nasa.gov/, accessed on 7 June 2021). The data with 1 km spatial resolution is a daily terrestrial atmospheric aerosol product generated by MODIS and a multi-angle atmospheric correction algorithm. It is featured with wider coverage and higher spatial and temporal resolution compared with other AOD products. Both MODIS instruments onboard the Terra and Aqua spacecraft provide daily AOD measurements [32]. To maximize the availability of AOD values, the combined values of Terra and Aqua were used to explore the spatial and temporal distribution patterns of AOD in East Asia.

2.1.2. DEM

The Digital Elevation Model (DEM) data used in this study is the Global Multi-Resolution Terrain Elevation Data (GMTED) from 2010, with a 200 m spatial resolution. We downloaded the data from the USGS and the NGA of the United States National Geological and Geographic Information Service (https://topotools.cr.usgs.gov/gmted_viewer/viewer.htm, accessed on 15 May 2021).

2.2. Statistical Methods

2.2.1. Linear Regression Trend Analysis

In this study, the linear tendency estimation method is used to analyze the long-term trend of the AOD at each pixel from 2011 to 2020. The X-axis is the year (time series), the Y-axis is the AOD, and the slope of the linear regression equation ($y = kx + b$), represents the tendency rate. When $k > 0$, the result indicates that the AOD exhibits a trend of growth, and vice versa. The formula for calculating the k is as follows:

$$k = (n\sum_{i=1}^{n} iX_i - \sum_{i=1}^{n} i \sum_{n}^{n} X_i) / \left[n\sum_{i=1}^{n} i^2 - (\sum_{i=1}^{n} i)^2 \right] \quad (1)$$

In the formula, n is the number of years (i.e., 10 in this study); i is the ith year (i.e., 2011 is the first year); and X_i is the annual average value of the AOD in the ith year.

2.2.2. Fitting Model

To better show the association between AOD and elevation, we used five fitting models to detect the variation of AOD with elevation, including linear, quadratic polynomial, logarithmic, exponential, and power functions.

To evaluate the goodness-of-fit more reasonably, the error sum of squares (SSE) and R-squared (R^2) are applied here. SSE is the error between the predicted value and the original value (MCD19A2 AOD). The size of SSE can be used to indicate how well the function is fitted. When the value of SSE is smaller, the fit is better. The opposite is worse. The calculation of SSE is shown in Equation (2).

$$SSE = \sum_{i=1}^{n} (y_i - \hat{y}_i)^2 \tag{2}$$

R^2 is used to indicate the model's goodness-of-fit, with values ranging from 0 to 1. R^2 is calculated from the sum of squared residuals (SSR) and the sum of squared total (SST). The closer R^2 is to 1, the better the model fit is. The calculation of R^2 is shown in Equation (5).

$$SSR = \sum_{i=1}^{n} (\hat{y}_i - \overline{y})^2 \tag{3}$$

$$SST = SSE + SSR = \sum_{i=1}^{n} (y_i - \overline{y})^2 \tag{4}$$

$$R^2 = \frac{SSR}{SST} = 1 - \frac{SSE}{SST} = 1 - \sum_{i=1}^{n} (y_i - \hat{y}_i)^2 / \sum_{i=1}^{n} (y_i - \overline{y})^2 \tag{5}$$

In Equations (2)–(5), i denotes the ith data; y_i and $\hat{y}_i$ denote the true and fitted values of the ith AOD, respectively; and $\overline{y}$ is the mean of the true AOD values.

3. Results and Discussion

3.1. Interannual Variation of AOD

Figure 2 shows the annual pattern of AOD in East Asia from 2011 to 2020. AOD in East Asia fluctuates between 0.203 and 0.246 from 2011 to 2020, with a mean value of 0.228. Since 2011, AOD in East Asia has been spiraling downward. The annual average AOD decreased by 0.034 (from 0.244 to 0.210), with an overall decrease of 14.029%. This indicates a significant improvement in atmospheric conditions.

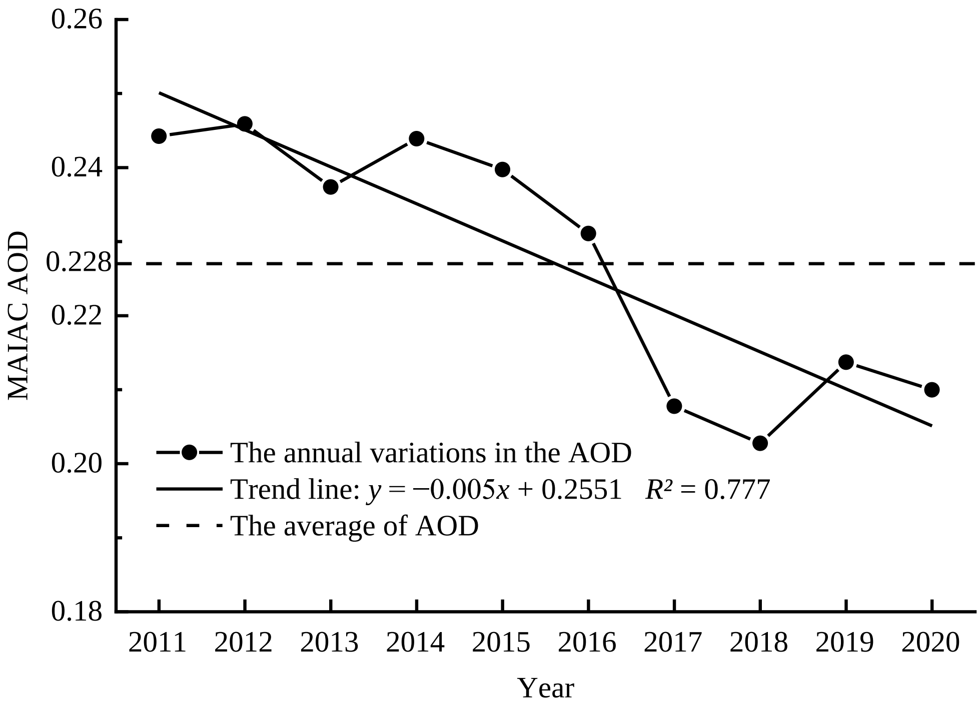

Figure 2. Year-to-year variation of the area-averaged AOD in East Asia from 2011 to 2020.

The spatial distribution of AOD varies considerably in different regions of East Asia (Figure 3). The distribution of AOD varies along with natural geographical conditions and human activities. The AOD values are lower than 0.2 in the Qinghai–Tibet Plateau and the areas north of 40° N. There are several reasons for the low AOD value in these regions. First, aerosols are mainly from local emissions, with little influence from dusty weather and surrounding transport in these areas [33]. Second, the population density is low, and there are few anthropogenic activities. The areas with high AOD values over 0.5 are mainly concentrated in the North China Plain area, the Sichuan Basin area, and the Ganges Delta area. Low and flat topography, a dense population, a high intensity of human activities, emissions of surface pollutants, and climate change in recent years are the main factors contributing to the high AOD values in these areas [34].

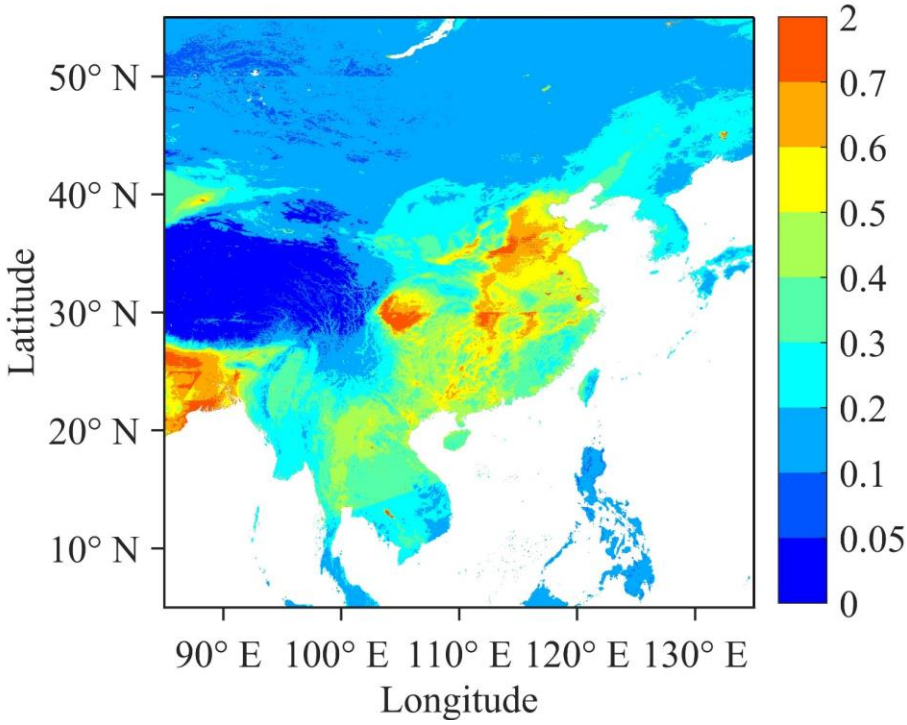

Figure 3. Spatial distribution of the AOD in East Asia averaged from 2011 to 2020.

The variation of the mean AOD values with altitude in East Asia shows that there is a significant difference in AOD values at different altitudes over the last 10 years (Figure 4). The mean AOD values at low altitudes are significantly higher than those at high altitudes, mainly due to the fact that low terrain makes aerosols less diffusible [35]. It also shows the ecological barrier role of higher altitude areas in resisting aerosols. Moreover, it shows that the centers of high AOD values are generally located in places with high population concentrations, developed economies, and lower elevations [36]. To explore the association between AOD and altitude from 2011 to 2020, we fitted them using different fitting models (Table 1). Under the five different fitting models, the results show that all the fitting curves have a good fitting effect except for the power fitting curve. Among them, the logarithmic function is the best model, with an R^2 of 0.9210 and SSE of 0.0245. It indicates that the distribution of AOD shows a logarithmic decreasing trend with increasing altitude in East Asia. Meanwhile, the lower the altitude, the faster the rate of AOD change with altitude (Figure 4).

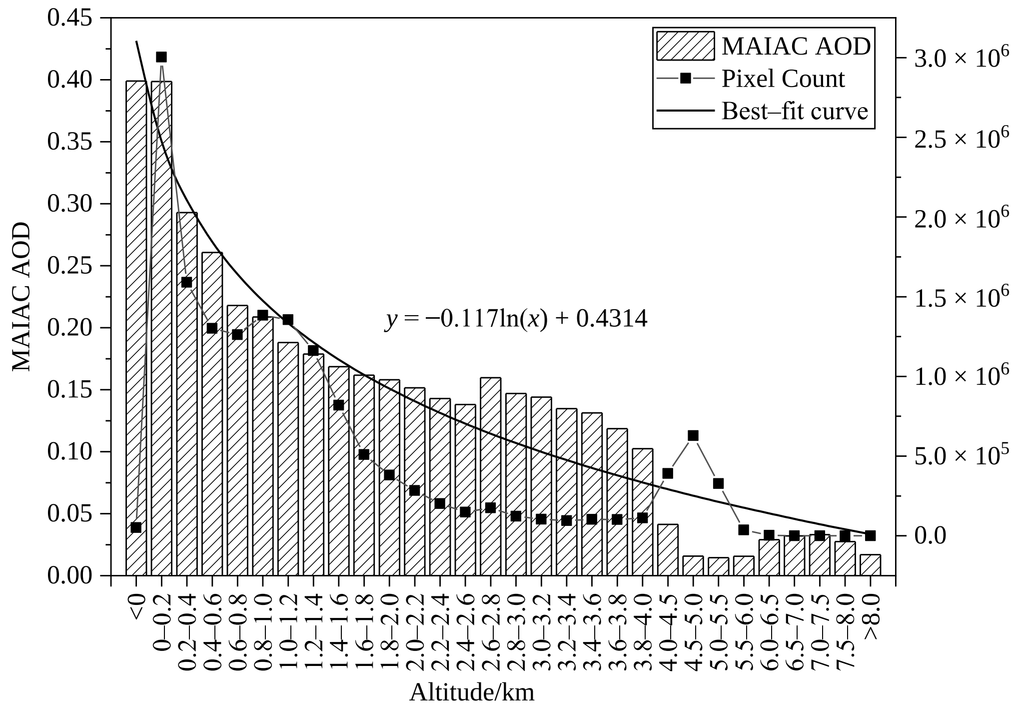

Figure 4. Variation of mean AOD with altitude over East Asia from 2011 to 2020 (Pixel Count is the number of image elements).

Table 1. Five different fitting models between AOD and altitude.

Fitting Model	Fitting Equation	R^2	SSE
Linear	$y = -0.0108x + 0.309$	0.8511	0.0462
Quadratic polynomial	$y = 0.0003x^2 - 0.0199x + 0.3574$	0.8883	0.0350
Logarithmic	$y = -0.117\ln(x) + 0.4314$	0.9210	0.0245
Exponential	$y = 0.4812e^{-0.104x}$	0.8078	0.0456
Power	$y = 1.0083x^{-0.942}$	0.6242	0.4470

As shown in Figure 2, the annual area-averaged AOD shows an approximately standard symmetrical "M" curve from 2011 to 2015, and the trend is down–up–down from 2016 to 2020 in East Asia. We compared the spatial distribution patterns of the AOD each year (Figure 5). Overall, there is a general decline in AOD values in Eastern Asia. The eastern and southeastern regions of China, as well as the Sichuan basin, exhibited higher AOD values from 2011 to 2015. The AOD values decreased significantly in these regions subsequently, which is consistent with the trend we identified in Figure 2. Previous studies revealed that the main aerosol types in East Asia are sulfate and dust [37]. The emission of sulfur dioxide in China has been decreasing year by year [38], which may have resulted in the decrease in AOD in this region. In contrast, aerosol pollution was higher in regions such as India and Bangladesh in the last decade [39]. Related studies have shown that South Asia is often considered one of the globally important aerosol hotspots [40–42]. In addition, the AOD values in Southeast Asia, mainly in Laos and Thailand, changed more significantly, which is related to the large-scale biomass-burning activities in Southeast Asia [43].

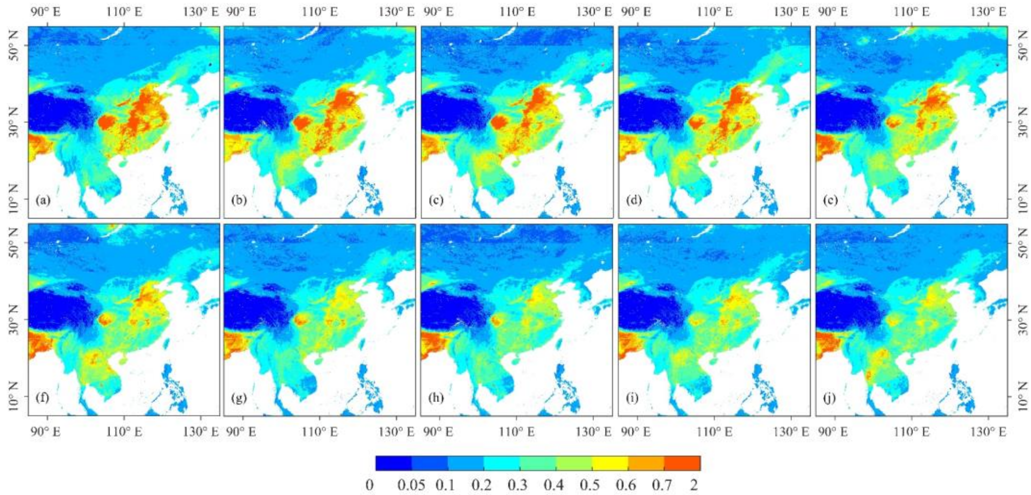

Figure 5. Annual spatial patterns of the AOD in East Asia from 2011 to 2020: (**a**) 2011, (**b**) 2012, (**c**) 2013, (**d**) 2014, (**e**) 2015, (**f**) 2016, (**g**) 2017, (**h**) 2018, (**i**) 2019, and (**j**) 2020.

It shows the spatial trends of AOD in East Asia in the last decade (Figure 6, Table 2). The results indicate that most areas of East Asia exhibited a decreasing trend in AOD from 2011 to 2020. The trends of AOD in East Asia differ considerably. More than 74% of this study area shows a decreasing trend in AOD, indicating a significant improvement in the environmental conditions in East Asia. The rate of AOD decrease is greater than 0.01 in the eastern and southeastern regions of China, and the fastest rate of AOD decrease is greater than 0.05 in the Sichuan basin. It proves that China has produced effective progress in energy conservation and emission reduction in recent years. In contrast, parts of South Asia and Southeast Asia are strongly influenced by human activities due to their large populations. Meanwhile, aerosol concentrations are influenced by meteorological conditions [35] and natural disasters [44], leading to an increase in AOD values in the areas.

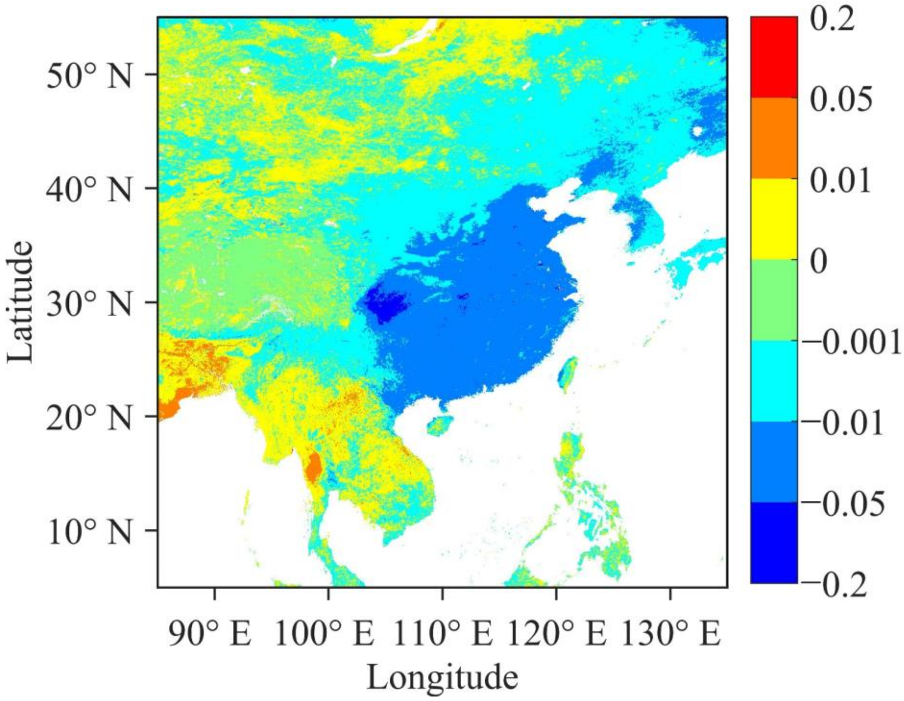

Figure 6. Spatial trends of AOD in East Asia from 2011 to 2020.

Table 2. Percentage share of AOD trends in East Asia from 2011 to 2020.

K	Percentage (%)	Trend	Total (%)
−0.2~−0.05	0.502	Decrease	74.627
−0.05~−0.01	17.291		
−0.01~−0.001	38.478		
−0.001~0	18.355		
0~0.001	24.071	Increase	25.373
0.001~0.05	1.299		
0.05~0.2	0.003		

3.2. Intra-Annual Variations of AOD

To better explore the monthly and seasonal variations of AOD in East Asia, the region is divided into four seasons: spring, summer, autumn, and winter. The four seasons are from March to May, June to August, September to November, and December to the following January and February, respectively.

The maximum, minimum, and mean values of AOD in East Asia are much higher in spring and summer than those in autumn and winter (Table 3). The average AOD in East Asia over the past 10 years is 0.282 and 0.244 in spring and summer, while the average AOD in autumn and winter is 0.184 and 0.211, respectively. There is a high possibility for dusty weather when dry conditions and relatively strong winds combine in the spring. Dust aerosols have a strong influence on spring aerosols [45]. These lead to larger aerosol concentrations in this region in the spring. Due to the hot and rainy climate during summer in most parts of this study area, high temperatures and high humidity further promote the formation of high aerosol concentrations [46]. The range of AOD in winter is slightly different from that in autumn. Compared to autumn, the relatively high AOD values in winter may be due to the coal or fossil fuel combustion for heating in winter in East Asia. The consumption of large amounts of coal and fossil fuels has released large amounts of industrial aerosols, which have an impact on the regional atmosphere and result in high AOD values. The largest decadal decreases in AOD values in East Asia are in summer and autumn, with 25.887% and 23.697%, respectively. During this period, the increased insolation levels cause significant warming over the land in East Asia [47]. Surface warming triggers an enhanced rise of warm air masses over the Asian continent. It invokes a strong transport of clean water vapor masses from the oceans into the interior of the Asian continent [48] and thus contributes to a decreased AOD [49]. Especially in summer and autumn, anthropogenic aerosols, which play a dominant role in East Asia, are an important factor in the weakening of the summer monsoon (July to September) in recent decades. During the period when anthropogenic aerosols are low, sulfate aerosols, etc., are also a major factor in the weakening trend of the monsoon [50]. The weakening of the Asian summer monsoon in turn severely affects the meteorological environment in East Asia, such as through reduced water vapor transport, which weakens aerosol concentrations [51].

The spatial patterns of AOD in different regions differ greatly across East Asia during the four seasons (Figures 7 and 8). Most regions have large seasonal variations in AOD. Because of numerous natural hazards and extreme weather in spring [52], the mean AOD in spring is higher in different parts of this study area. Among them, AOD values peak in Southeast Asia and Southeast China [43]. Biomass burning in Southeast Asia in spring can also affect aerosol concentrations in Southwest China and the Pearl River Delta region through long-range transport [53,54]. In contrast, the Tibetan Plateau region and areas north of 40° N have lower AOD values and variability. The South Asia region, mainly India and Bangladesh, maintains high AOD values throughout the seasons. The high aerosol contribution from natural emissions and local anthropogenic emissions is the main driver of high AOD in these regions for the four seasons [33,55]. The Qinghai–Tibet Plateau region maintains a low AOD value throughout the seasons. The reason is that the Qinghai–Tibet Plateau forms a natural barrier due to its high altitude and natural environment [39].

Table 3. Quarterly mean AOD in East Asia from 2011 to 2020.

Year	Spring	Summer	Autumn	Winter
2011	0.285	0.282	0.211	0.241
2012	0.324	0.277	0.185	0.215
2013	0.303	0.217	0.200	0.249
2014	0.310	0.281	0.198	0.183
2015	0.281	0.260	0.186	0.228
2016	0.298	0.222	0.184	0.203
2017	0.239	0.233	0.173	0.194
2018	0.261	0.218	0.158	0.186
2019	0.259	0.237	0.180	0.204
2020	0.259	0.209	0.161	0.209
Mean	0.282	0.244	0.184	0.211
Maximum	0.324	0.282	0.211	0.249
Minimum	0.239	0.209	0.158	0.183
Decreases of decade	0.026	0.073	0.050	0.032
Degree of decreases	9.123%	25.887%	23.697%	13.278%

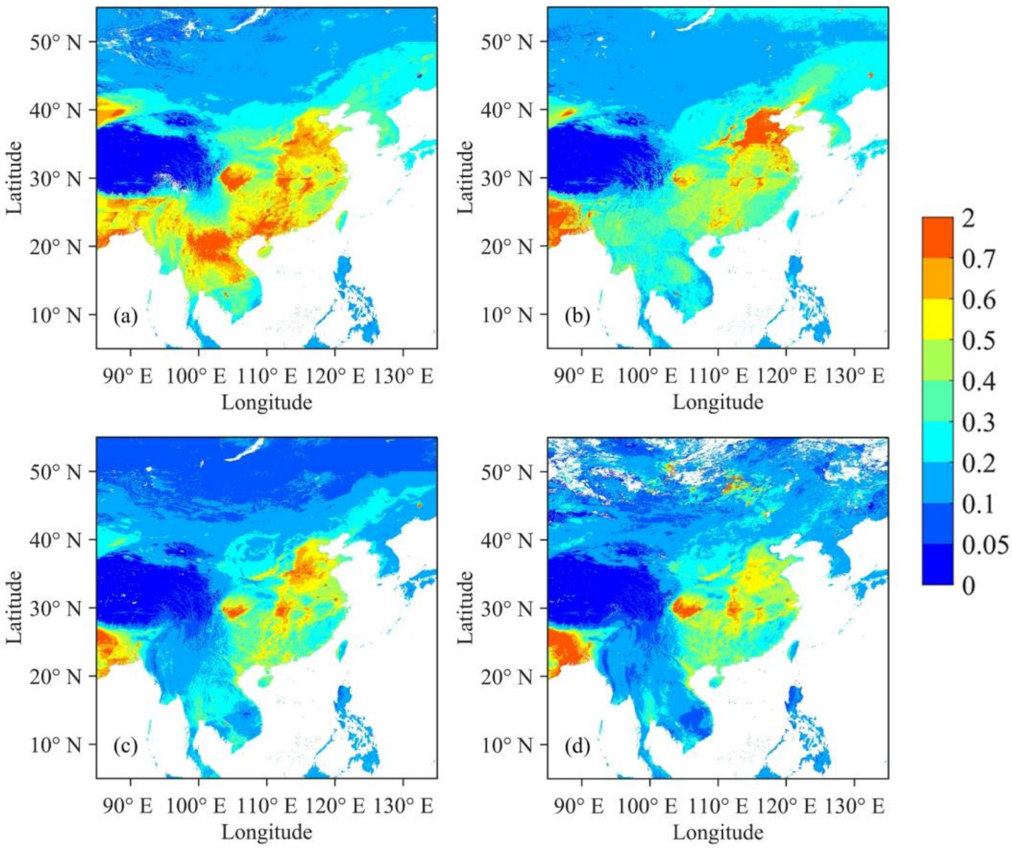

Figure 7. Seasonal mean AOD in East Asia from 2011 to 2020: (**a**) Spring, (**b**) Summer, (**c**) Autumn, and (**d**) Winter.

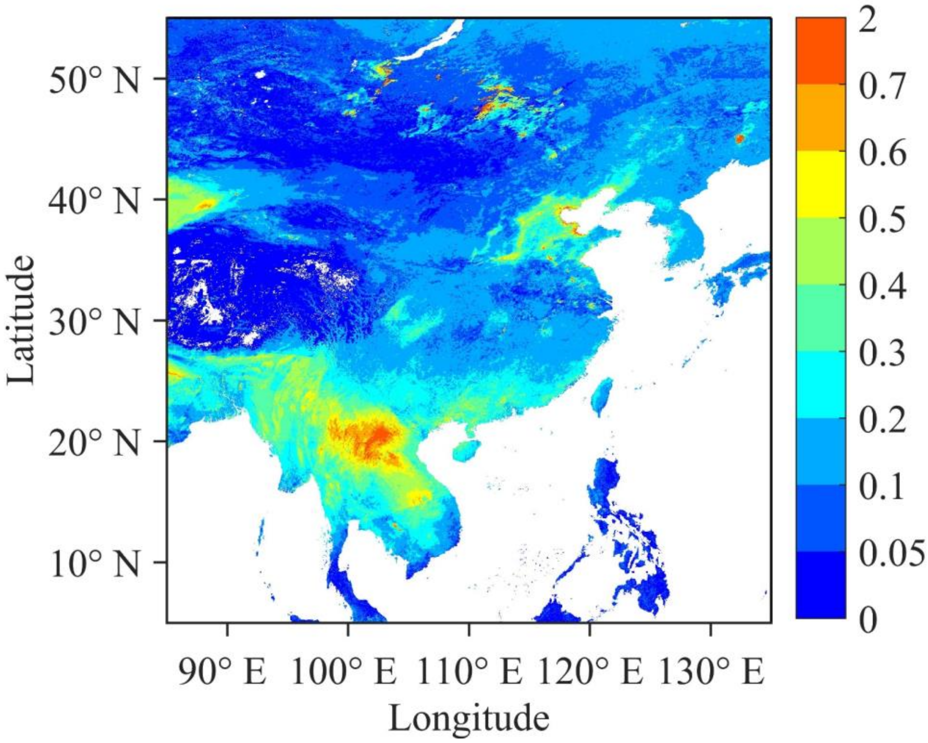

Figure 8. The magnitude of AOD variation in East Asia over the four seasons.

The monthly average AOD values from 2011 to 2020 were very different (Figure 9, Table 4). The monthly average of AOD has been 0.242 over the past decade. For different months, the AOD values peak at 0.326 in March and are as low as 0.189 in November. The monthly average of AOD from August to December is below the monthly average. It is possible because the frequent cold air activity accelerated the diffusion and transport of aerosol particles during this period [56]. From November to February, the AOD showed an increasing trend. Due to the demand for heating in the north and unfavorable meteorological conditions, severe haze pollution events are prone to occur [57,58]. The AOD values in East Asia show a continuous decreasing trend from March to September. The possible reason is the reduction in coal burning during the non-heating period. At the same time, the rainfall during the rainy season helps flush pollutants from the atmosphere [59]. From 2011 to 2020, the overall trend of monthly AOD values has decreased. However, the fluctuation of the monthly AOD is diverse, and the magnitude of the decline also varies greatly from month to month. In East Asia, April is during the period when cold and warm currents meet frequently, and its AOD values fluctuate most dramatically due to climate changes such as increased temperature and precipitation. In addition, fluctuations in AOD values during this period are influenced by fuel and biomass combustion and dust [60]. The largest decline is 33.840% in August and the smallest decline is 0.658% in March. Energy savings have led to a decrease in residentially and industrially generated aerosols.

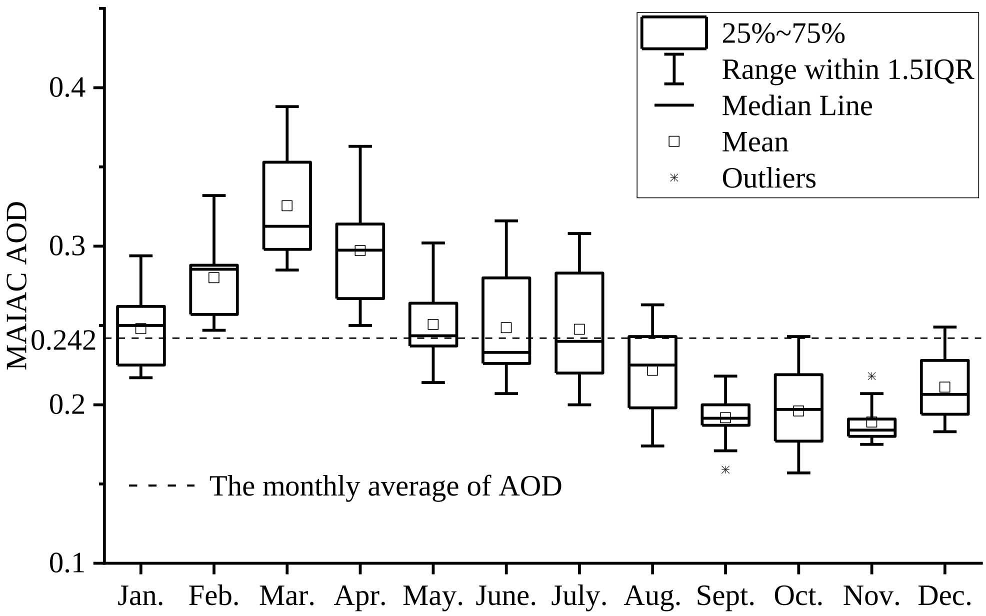

Figure 9. Monthly variation of AOD in East Asia from 2011 to 2020.

Table 4. Monthly average of AOD in East Asia from 2011 to 2020.

Month/Year	2011	2012	2013	2014	2015	2016	2017	2018	2019	2020	Mean	Decreases of Decade	Degree of Decreases
January	0.265	0.253	0.294	0.262	0.238	0.247	0.225	0.218	0.217	0.261	0.248	0.004	1.509%
February	0.332	0.273	0.291	0.288	0.285	0.287	0.257	0.255	0.247	0.286	0.280	0.046	13.855%
March	0.304	0.381	0.388	0.321	0.331	0.353	0.285	0.298	0.292	0.302	0.326	0.002	0.658%
April	0.314	0.306	0.324	0.363	0.299	0.295	0.250	0.267	0.258	0.296	0.297	0.018	5.732%
May	0.276	0.302	0.242	0.243	0.244	0.264	0.229	0.237	0.255	0.214	0.251	0.062	22.464%
June	0.280	0.316	0.235	0.293	0.226	0.231	0.256	0.227	0.215	0.207	0.249	0.073	26.071%
July	0.283	0.264	0.200	0.308	0.287	0.235	0.224	0.210	0.245	0.220	0.248	0.063	22.261%
August	0.263	0.241	0.214	0.236	0.251	0.201	0.196	0.198	0.243	0.174	0.222	0.089	33.840%
September	0.218	0.187	0.190	0.193	0.194	0.218	0.171	0.159	0.200	0.188	0.192	0.030	13.761%
October	0.219	0.199	0.243	0.223	0.197	0.189	0.197	0.157	0.177	0.159	0.196	0.060	27.397%
November	0.218	0.207	0.191	0.190	0.184	0.180	0.183	0.184	0.178	0.175	0.189	0.043	19.725%
December	0.241	0.215	0.249	0.183	0.228	0.202	0.194	0.186	0.204	0.209	0.211	0.032	13.278%

3.3. Spatiotemporal Variations of AOD in High and Low Hotspots

According to Figure 3 and Table 5, it shows that relatively high values of AOD are concentrated in the North China Plain, the Sichuan Basin, and the Ganges Delta. The highest mean values of AOD are found in the Sichuan basin and the Ganges Delta, with 0.514 and 0.527, respectively. In addition to local emissions, a significant portion of aerosols are transmitted from other regions due to the low altitude of the central Sichuan basin [61]. It is difficult to diffuse after aerosol aggregation, which easily leads to the accumulation of different types of aerosol particles in the Sichuan basin. The Ganges Delta is the largest delta in the world. Its large population, large-scale industrial and agricultural development, and natural disasters such as dust storms have led to persistently high AOD values in this region. In contrast, the annual average AOD values in the Qinghai–Tibet Plateau area are significantly lower. Due to the low population density in this area, the contribution of anthropogenic aerosols to AOD is small. The highest value of the quarterly AOD in the North China Plain occurs in summer. In addition to the major contributions made by anthropogenic aerosol [62,63] and long-range transported aerosol [64], the high water content in the atmosphere caused by the hot and rainy summers in the region and the hygroscopic nature of the aerosols promote the increase in AOD and the transformation of secondary aerosols [9]. The highest values of quarterly AOD in the Sichuan Basin, Ganges

Delta, and Tibetan Plateau all occur in spring, similar to the overall seasonal variation in East Asia.

Table 5. Yearly and quarterly averaged AOD in different regions of East Asia from 2011 to 2020.

Region	Annual Mean AOD	Seasonal Mean AOD			
		Spring	Summer	Autumn	Winter
North China Plain area	0.497	0.523	0.573	0.469	0.406
Sichuan Basin area	0.514	0.573	0.428	0.428	0.510
Ganges Delta area	0.527	0.569	0.535	0.438	0.519
Qinghai-Tibetan Plateau area	0.061	0.077	0.076	0.053	0.051

In the last decade, the annual variation of AOD in the three hot spots has been significantly different (Figure 10). In the last decade, AOD values in the Sichuan basin and the North China plain all decreased, while they increased in the Ganges delta. The AOD value of the Sichuan basin decreases by 0.317, a decrease of 45.14%. This region has the largest decrease in high values of AOD. There was a large aerosol accumulation in the Sichuan Basin in earlier years. After the effective implementation of China's environmental management policies in recent years, it has led to a significant decrease in AOD values in the Sichuan Basin [65]. The increasing trend in the Ganges Delta can be attributed to the increase in emissions from biomass burning (e.g., wood fuel and agricultural waste) [66]. Under the influence of human activities and the natural environment, there are pressing environmental problems in the Ganges Delta.

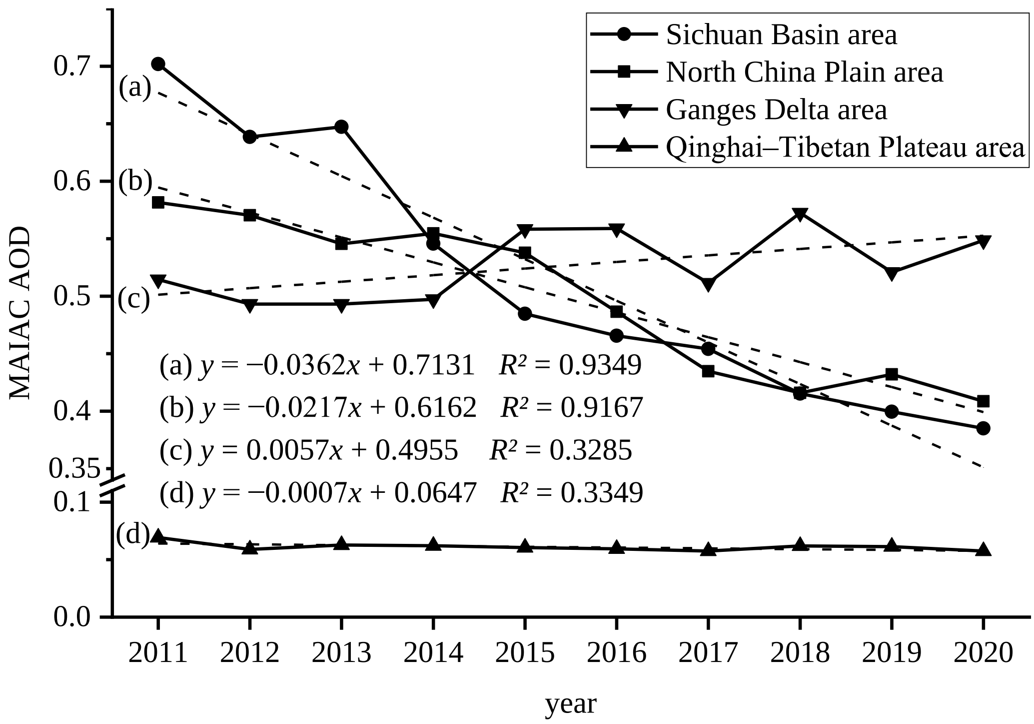

Figure 10. Variations of the AOD in different areas in East Asia from 2011 to 2020.

4. Conclusions

Through this study, it was found that the distribution of AOD in East Asia varied greatly. Overall, the average AOD value in East Asia in the last decade was 0.228. The high AOD areas were mainly distributed in the North China Plain region, the Sichuan Basin region, and the Ganges Delta region, while the low AOD areas were mainly distributed in the Qinghai–Tibet Plateau region. The obvious altitude characteristics of these regions prompted us to understand the association between AOD and altitude. It was found that the distribution of AOD showed a logarithmic decreasing trend with increasing altitude and that the rate of change of AOD was faster in low-altitude areas. This result made us clearer about the pattern of the spatial distribution of AOD in East Asia in terms of altitude.

By analyzing the spatial-temporal variation of AOD in East Asia, we found that the atmospheric environmental conditions in East Asia have significantly improved. Temporally, the decreasing trend of annual average AOD in East Asia is obvious in the last decade. Spatially, the AOD in most of East Asia is on a downward trend. Large areas, mainly including eastern and southeastern China, experienced a decline in AOD at a rate greater than 0.01, due to the effective implementation of China's energy conservation and emission reduction policies. The fastest decline in AOD values was in the Sichuan basin, which exceeded 0.05. In contrast, in India and parts of Southeast Asia, AOD values increased due to the impact of human activities, meteorological conditions, and natural disasters.

We explored the characteristics of its intra-annual variation through quarterly and monthly AOD analyses. The results showed that AOD values showed significant differences among the four seasons. The maximum, minimum, and mean AOD values were much higher in spring and summer than in autumn and winter due to the meteorological environment and anthropogenic activities. In terms of the spatial distribution of quarterly AOD, there are significant peaks in spring in Southeast Asia and Southeast China due to climate, biomass burning, and long-range transport. In the three typical areas of high AOD values in East Asia, the highest quarterly AOD values in the North China Plain occurred in summer. The highest quarterly AOD values in the Sichuan Basin, the Ganges Delta, and the Tibetan Plateau all occurred in spring, similar to the overall seasonal variation in East Asia. In terms of the monthly variation of AOD, it peaked in March and was lowest in November. During the period from March to September, AOD showed a continuous decreasing trend. This is generally consistent with the distribution pattern of the quarterly AOD.

Author Contributions: Conceptualization, Q.T.; methodology, P.W. and Q.T.; software, P.W. and Q.T.; validation, Q.T.; formal analysis, P.W.; investigation, P.W. and Q.T.; resources, P.W.; data curation, P.W. and Q.T.; writing—original draft preparation, P.W.; writing—review and editing, P.W., Q.T., Y.Z., Y.H., K.Z., T.L. and Q.Y.; visualization, P.W.; supervision, Q.T.; project administration, Q.T.; funding acquisition, Q.T., T.L. and Q.Y. All authors have read and agreed to the published version of the manuscript.

Funding: This research was funded by the National Natural Science Foundation of China, grant numbers 31800367 and 41971025, and the Natural Foundation of Shandong Province of China, grant numbers ZR2021MD090 and ZR2017MD017.

Institutional Review Board Statement: Not applicable.

Informed Consent Statement: Not applicable.

Data Availability Statement: The MCD19A2 dataset is available at the National Aeronautics and Space Administration (NASA) Goddard Space Flight Center (https://earthdata.nasa.gov/, accessed on 7 June 2021). GMTED for 2010 is available from the USGS and the NGA of the United States National Geological and Geographic Information Service (https://topotools.cr.usgs.gov/gmted_viewer/viewer.htm, accessed on 15 May 2021).

Acknowledgments: We would like to thank the NASA Earth Data website (https://search.earthdata.nasa.gov/search) for providing MODIS aerosol products.

Conflicts of Interest: The authors declare no conflict of interest.

References

1. Xin, J.; Zhang, Q.; Wang, L.; Gong, C.; Wang, Y.; Liu, Z.; Gao, W. The empirical relationship between the PM2.5 concentration and aerosol optical depth over the background of North China from 2009 to 2011. *Atmos. Res.* **2014**, *138*, 179–188. [CrossRef]
2. Wang, J.; Wu, J.; Liu, B.; Liu, X.; Gao, H.; Zhang, Y.; Feng, Y.; Han, S.; Gong, X. Exploring the Sensitivity of Visibility to PM2.5 Mass Concentration and Relative Humidity for Different Aerosol Types. *Atmosphere* **2022**, *13*, 471. [CrossRef]

3. Lacagnina, C.; Hasekamp, O.P.; Torres, O. Direct radiative effect of aerosols based on PARASOL and OMI satellite observations. *J. Geophys. Res. Atmos.* **2017**, *122*, 2366–2388. [CrossRef]
4. Tsui, W.G.; Woo, J.L.; McNeill, V.F. Impact of Aerosol-Cloud Cycling on Aqueous Secondary Organic Aerosol Formation. *Atmosphere* **2019**, *10*, 666. [CrossRef]
5. Luo, R.; Liu, Y.; Zhu, Q.; Tang, Y.; Shao, T. Effects of aerosols on cloud and precipitation in East-Asian drylands. *Int. J. Climatol.* **2021**, *41*, 4603–4618. [CrossRef]
6. Madadi, A.; Sadr, A.H.; Kashani, A.; Gilandeh, A.G.; Safarianzengir, V.; Kianian, M. Monitoring of aerosols and studying its effects on the environment and humans health in Iran. *Environ. Geochem. Health* **2021**, *43*, 317–331. [CrossRef]
7. Okuda, T.; Schauer, J.J.; Shafer, M.M. Improved methods for elemental analysis of atmospheric aerosols for evaluating human health impacts of aerosols in East Asia. *Atmos. Environ.* **2014**, *97*, 552–555. [CrossRef]
8. Al-Salihi, A.M. Characterization of aerosol type based on aerosol optical properties over Baghdad, Iraq. *Arab. J. Geosci.* **2018**, *11*, 633. [CrossRef]
9. Zhao, H.; Che, H.; Xia, X.; Wang, Y.; Wang, H.; Wang, P.; Ma, Y.; Yang, H.; Liu, Y.; Wang, Y.; et al. Multiyear Ground-Based Measurements of Aerosol Optical Properties and Direct Radiative Effect Over Different Surface Types in Northeastern China. *J. Geophys. Res. Atmos.* **2018**, *123*, 13887–13916. [CrossRef]
10. Pappalardo, G.; Amodeo, A.; Apituley, A.; Comeron, A.; Freudenthaler, V.; Linné, H.; Ansmann, A.; Bösenberg, J.; D'Amico, G.; Mattis, I.; et al. EARLINET: Towards an advanced sustainable European aerosol lidar network. *Atmos. Meas. Tech.* **2014**, *7*, 2389–2409. [CrossRef]
11. Kittaka, C.; Winker, D.M.; Vaughan, M.A.; Omar, A.; Remer, L.A. Intercomparison of column aerosol optical depths from CALIPSO and MODIS-Aqua. *Atmos. Meas. Tech.* **2011**, *4*, 131–141. [CrossRef]
12. Wang, W.; Mao, F.; Pan, Z.; Du, L.; Gong, W. Validation of VIIRS AOD through a Comparison with a Sun Photometer and MODIS AODs over Wuhan. *Remote Sens.* **2017**, *9*, 403. [CrossRef]
13. Jin, Y.; Hao, Z.; Chen, J.; He, D.; Tian, Q.; Mao, Z.; Pan, D. Retrieval of Urban Aerosol Optical Depth from Landsat 8 OLI in Nanjing, China. *Remote Sens.* **2021**, *13*, 415. [CrossRef]
14. Li, J.; He, Q.; Ge, X.; Abbas, A. Spatiotemporal distribution of aerosols over the Tibet Plateau and Tarim Basin (1980–2020). *J. Clean. Prod.* **2022**, *374*, 133958. [CrossRef]
15. Wang, W.; Zhu, D.; Jing, C.; Guo, X.; Chen, L. Spatial distribution and temporal variation of aerosol optical depth in the Western Pacific Ocean. *Dyn. Atmos. Ocean.* **2022**, *99*, 101303. [CrossRef]
16. Kaufman, Y.J.; Tanré, D.; Remer, L.A.; Vermote, E.F.; Chu, A.; Holben, B.N. Operational remote sensing of tropospheric aerosol over land from EOS moderate resolution imaging spectroradiometer. *J. Geophys. Res. Atmos.* **1997**, *102*, 17051–17067. [CrossRef]
17. Levy, R.C.; Mattoo, S.; Munchak, L.A.; Remer, L.A.; Sayer, A.M.; Patadia, F.; Hsu, N.C. The Collection 6 MODIS aerosol products over land and ocean. *Atmos. Meas. Tech.* **2013**, *6*, 2989–3034. [CrossRef]
18. Hsu, N.C.; Jeong, M.J.; Bettenhausen, C.; Sayer, A.M.; Hansell, R.; Seftor, C.S.; Huang, J.; Tsay, S.C. Enhanced Deep Blue aerosol retrieval algorithm: The second generation. *J. Geophys. Res. Atmos.* **2013**, *118*, 9296–9315. [CrossRef]
19. Wang, Y.; Wang, J.; Levy, R.C.; Shi, Y.R.; Mattoo, S.; Reid, J.S. First Retrieval of AOD at Fine Resolution Over Shallow and Turbid Coastal Waters From MODIS. *Geophys. Res. Lett.* **2021**, *48*, e2021GL094344. [CrossRef]
20. Cheng, L.; Li, L.; Chen, L.; Hu, S.; Yuan, L.; Liu, Y.; Cui, Y.; Zhang, T. Spatiotemporal Variability and Influencing Factors of Aerosol Optical Depth over the Pan Yangtze River Delta during the 2014–2017 Period. *Int. J. Environ. Res. Public Health* **2019**, *16*, 3522. [CrossRef]
21. Shen, X.; Bilal, M.; Qiu, Z.; Sun, D.; Wang, S.; Zhu, W. Long-term spatiotemporal variations of aerosol optical depth over Yellow and Bohai Sea. *Environ. Sci. Pollut. Res. Int.* **2019**, *26*, 7969–7979. [CrossRef] [PubMed]
22. Boiyo, R.; Kumar, K.R.; Zhao, T. Spatial variations and trends in AOD climatology over East Africa during 2002-2016: A comparative study using three satellite data sets. *Int. J. Climatol.* **2018**, *38*, e1221–e1240. [CrossRef]
23. Lyapustin, A.; Wang, Y.; Korkin, S.; Huang, D. MODIS Collection 6 MAIAC algorithm. *Atmos. Meas. Tech.* **2018**, *11*, 5741–5765. [CrossRef]
24. Mhawish, A.; Banerjee, T.; Sorek-Hamer, M.; Lyapustin, A.; Broday, D.M.; Chatfield, R. Comparison and evaluation of MODIS Multi-angle Implementation of Atmospheric Correction (MAIAC) aerosol product over South Asia. *Remote Sens. Environ.* **2019**, *224*, 12–28. [CrossRef]
25. Soleimany, A.; Solgi, E.; Ashrafi, K.; Jafari, R.; Grubliauskas, R. Temporal and spatial distribution mapping of particulate matter in southwest of Iran using remote sensing, GIS, and statistical techniques. *Air Qual. Atmos. Health* **2022**, *15*, 1057–1078. [CrossRef]
26. Dong, J.; Wang, X.; Li, J.; Hao, C.; Jiao, L. The Spatial-Temporal Differentiation of Aerosol Optical Properties and Types in the Beijing–Tianjin–Hebei Region Based on the Ecological Functional Zones. *Sustainability* **2022**, *14*, 12656. [CrossRef]
27. Bi, J.; Huang, J.; Holben, B.; Zhang, G. Comparison of key absorption and optical properties between pure and transported anthropogenic dust over East and Central Asia. *Atmos. Chem. Phys.* **2016**, *16*, 15501–15516. [CrossRef]
28. Kumar, D.B.; Verma, S. Potential emission flux to aerosol pollutants over Bengal Gangetic plain through combined trajectory clustering and aerosol source fields analysis. *Atmos. Res.* **2016**, *178–179*, 415–425. [CrossRef]
29. Lau, K.M.; Ramanathan, V.; Wu, G.X.; Li, Z.; Tsay, S.C.; Hsu, C.; Sikka, R.; Holben, B.; Lu, D.; Tartari, G.; et al. The Joint Aerosol–Monsoon Experiment: A New Challenge for Monsoon Climate Research. *Bull. Am. Meteorol. Soc.* **2008**, *89*, 369–384. [CrossRef]

30. Giri, B.; Patel, K.S.; Jaiswal, N.K.; Sharma, S.; Ambade, B.; Wang, W.; Simonich, S.L.M.; Simoneit, B.R.T. Composition and sources of organic tracers in aerosol particles of industrial central India. *Atmos. Res.* **2013**, *120–121*, 312–324. [CrossRef]
31. Ramachandran, S.; Srivastava, R. Mixing states of aerosols over four environmentally distinct atmospheric regimes in Asia: Coastal, urban, and industrial locations influenced by dust. *Environ. Sci. Pollut. Res. Int.* **2016**, *23*, 11109–11128. [CrossRef] [PubMed]
32. Jung, C.R.; Hwang, B.F.; Chen, W.T. Incorporating long-term satellite-based aerosol optical depth, localized land use data, and meteorological variables to estimate ground-level PM2.5 concentrations in Taiwan from 2005 to 2015. *Environ. Pollut.* **2018**, *237*, 1000–1010. [CrossRef] [PubMed]
33. Liu, B.; Cong, Z.; Wang, Y.; Xin, J.; Wan, X.; Pan, Y.; Liu, Z.; Wang, Y.; Zhang, G.; Wang, Z.; et al. Background aerosol over the Himalayas and Tibetan Plateau: Observed characteristics of aerosol mass loading. *Atmos. Chem. Phys.* **2017**, *17*, 449–463. [CrossRef]
34. Huang, C.; Li, J.; Sun, W.; Chen, Q.; Mao, Q.-J.; Yuan, Y. Long-Term Variation Assessment of Aerosol Load and Dominant Types over Asia for Air Quality Studies Using Multi-Sources Aerosol Datasets. *Remote Sens.* **2021**, *13*, 3116. [CrossRef]
35. Wang, D.; Zhang, F.; Yang, S.; Xia, N.; Ariken, M. Exploring the spatial-temporal characteristics of the aerosol optical depth (AOD) in Central Asia based on the moderate resolution imaging spectroradiometer (MODIS). *Environ. Monit. Assess.* **2020**, *192*, 383. [CrossRef]
36. Wang, Y.; Yu, X.; Xie, G. Spatial distribution and temporal variation of aerosol optical depth over China in the past 15 years. *China Environ. Sci.* **2018**, *38*, 426–434. [CrossRef]
37. Hu, Z.; Zhao, C.; Huang, J.; Leung, L.R.; Qian, Y.; Yu, H.; Huang, L.; Kalashnikova, O.V. Trans-Pacific transport and evolution of aerosols: Evaluation of quasi-global WRF-Chem simulation with multiple observations. *Geosci. Model Dev.* **2016**, *9*, 1725–1746. [CrossRef]
38. Lu, Z.; Streets, D.G.; Zhang, Q.; Wang, S.; Carmichael, G.R.; Cheng, Y.F.; Wei, C.; Chin, M.; Diehl, T.; Tan, Q. Sulfur dioxide emissions in China and sulfur trends in East Asia since 2000. *Atmos. Chem. Phys.* **2010**, *10*, 6311–6331. [CrossRef]
39. Zhang, M.; Wang, L.; Bilal, M.; Gong, W.; Zhang, Z.; Guo, G. The Characteristics of the Aerosol Optical Depth within the Lowest Aerosol Layer over the Tibetan Plateau from 2007 to 2014. *Remote Sens.* **2018**, *10*, 696. [CrossRef]
40. Singh, N.; Murari, V.; Kumar, M.; Barman, S.C.; Banerjee, T. Fine particulates over South Asia: Review and meta-analysis of PM2.5 source apportionment through receptor model. *Environ. Pollut.* **2017**, *223*, 121–136. [CrossRef]
41. Saikawa, E.; Wu, Q.; Zhong, M.; Avramov, A.; Ram, K.; Stone, E.A.; Stockwell, C.E.; Jayarathne, T.; Panday, A.K.; Yokelson, R.J. Garbage Burning in South Asia: How Important Is It to Regional Air Quality? *Environ. Sci. Technol.* **2020**, *54*, 9928–9938. [CrossRef] [PubMed]
42. Gautam, R.; Hsu, N.C.; Tsay, S.C.; Lau, K.M.; Holben, B.; Bell, S.; Smirnov, A.; Li, C.; Hansell, R.; Ji, Q.; et al. Accumulation of aerosols over the Indo-Gangetic plains and southern slopes of the Himalayas: Distribution, properties and radiative effects during the 2009 pre-monsoon season. *Atmos. Chem. Phys.* **2011**, *11*, 12841–12863. [CrossRef]
43. Wu, J.; Fu, C. Simulation Research of Distribution Transportation and Radiative Effects of Black Carbon Aerosol in Recent Five Spring Seasons over East Asia Region. *Chin. J. Atmos. Sci.* **2005**, *29*, 111–119.
44. Cohen, J.B.; Lecoeur, E.; Hui Loong Ng, D. Decadal-scale relationship between measurements of aerosols, land-use change, and fire over Southeast Asia. *Atmos. Chem. Phys.* **2017**, *17*, 721–743. [CrossRef]
45. Xia, X.; Che, H.; Zhu, J.; Chen, H.; Cong, Z.; Deng, X.; Fan, X.; Fu, Y.; Goloub, P.; Jiang, H.; et al. Ground-based remote sensing of aerosol climatology in China: Aerosol optical properties, direct radiative effect and its parameterization. *Atmos. Environ.* **2016**, *124*, 243–251. [CrossRef]
46. Yli-Juuti, T.; Mielonen, T.; Heikkinen, L.; Arola, A.; Ehn, M.; Isokaanta, S.; Keskinen, H.M.; Kulmala, M.; Laakso, A.; Lipponen, A.; et al. Significance of the organic aerosol driven climate feedback in the boreal area. *Nat. Commun.* **2021**, *12*, 5637. [CrossRef]
47. Zhou, B.; Zhao, P. Inverse correlation between ancient winter and summer monsoons in East Asia? *Chin. Sci. Bull.* **2009**, *54*, 3760–3767. [CrossRef]
48. Kaboth-Bahr, S.; Bahr, A.; Zeeden, C.; Yamoah, K.A.; Lone, M.A.; Chuang, C.-K.; Löwemark, L.; Wei, K.-Y. A tale of shifting relations: East Asian summer and winter monsoon variability during the Holocene. *Sci. Rep.* **2021**, *11*, 6938. [CrossRef]
49. Kim, D.; Chin, M.; Yu, H.; Diehl, T.; Tan, Q.; Kahn, R.A.; Tsigaridis, K.; Bauer, S.E.; Takemura, T.; Pozzoli, L.; et al. Sources, sinks, and transatlantic transport of North African dust aerosol: A multimodel analysis and comparison with remote sensing data. *J. Geophys. Res. Atmos.* **2014**, *119*, 6259–6277. [CrossRef]
50. Liu, Y.; Cai, W.; Sun, C.; Song, H.; Cobb, K.M.; Li, J.; Leavitt, S.W.; Wu, L.; Cai, Q.; Liu, R.; et al. Anthropogenic Aerosols Cause Recent Pronounced Weakening of Asian Summer Monsoon Relative to Last Four Centuries. *Geophys. Res. Lett.* **2019**, *46*, 5469–5479. [CrossRef]
51. Liu, H.; Miao, J.; Wu, K.; Du, M.; Zhu, Y.; Hou, S. Why the Increasing Trend of Summer Rainfall over North China Has Halted since the Mid-1990s. *Adv. Meteorol.* **2020**, *2020*, 9031796. [CrossRef]
52. Lee, S.; Lee, M.I.; Song, C.K.; Kim, K.M.; da Silva, A.M. Interannual Variation of the East Asia Jet Stream and Its Impact on the Horizontal Distribution of Aerosol in Boreal Spring. *Atmos. Environ. (1994)* **2020**, *223*, 117296. [CrossRef] [PubMed]
53. Deng, X.; Tie, X.; Zhou, X.; Wu, D.; Zhong, L.; Tan, H.; Li, F.; Huang, X.; Bi, X.; Deng, T. Effects of Southeast Asia biomass burning on aerosols and ozone concentrations over the Pearl River Delta (PRD) region. *Atmos. Environ.* **2008**, *42*, 8493–8501. [CrossRef]

54. Hansen, A.B.; Witham, C.S.; Chong, W.M.; Kendall, E.; Chew, B.N.; Gan, C.; Hort, M.C.; Lee, S.-Y. Haze in Singapore-source attribution of biomass burning PM₁₀ from Southeast Asia. *Atmos. Chem. Phys.* **2019**, *19*, 5363–5385. [CrossRef]
55. Mhawish, A.; Sorek-Hamer, M.; Chatfield, R.; Banerjee, T.; Bilal, M.; Kumar, M.; Sarangi, C.; Franklin, M.; Chau, K.; Garay, M.; et al. Aerosol characteristics from earth observation systems: A comprehensive investigation over South Asia (2000–2019). *Remote Sens. Environ.* **2021**, *259*, 112410. [CrossRef]
56. Caixia, Y.; Chun'e, S.; Xinfeng, L.; Yuejia, Z.; Wei, F. Analysis of a severe fog-haze process in central and eastern China based on comprehensive observations. *Acta Sci. Circumstantiae* **2020**, *40*, 2346–2355. [CrossRef]
57. Wu, C.; Wang, G.; Wang, J.; Li, J.; Ren, Y.; Zhang, L.; Cao, C.; Li, J.; Ge, S.; Xie, Y.; et al. Chemical characteristics of haze particles in Xi'an during Chinese Spring Festival: Impact of fireworks burning. *J. Environ. Sci.* **2018**, *71*, 179–187. [CrossRef]
58. Wang, G.; Zhang, F.; Peng, J.; Duan, L.; Ji, Y.; Marrero-Ortiz, W.; Wang, J.; Li, J.; Wu, C.; Cao, C.; et al. Particle acidity and sulfate production during severe haze events in China cannot be reliably inferred by assuming a mixture of inorganic salts. *Atmos. Chem. Phys.* **2018**, *18*, 10123–10132. [CrossRef]
59. Filonchyk, M.; Yan, H.; Zhang, Z.; Yang, S.; Li, W.; Li, Y. Combined use of satellite and surface observations to study aerosol optical depth in different regions of China. *Sci. Rep.* **2019**, *9*, 6174. [CrossRef]
60. Nam, J.; Kim, S.-W.; Park, R.J.; Park, J.-S.; Park, S.S. Changes in column aerosol optical depth and ground-level particulate matter concentration over East Asia. *Air Qual. Atmos. Health* **2017**, *11*, 49–60. [CrossRef]
61. Liao, Y.; Yang, F.; Luo, Y.; Zhao, T.; Shang, Y.; Zheng, X. Regional Climatology of Aerosol Distribution over Yunnan-Guizhou Plateau. *Ecol. Environ. Sci.* **2019**, *28*, 316–323. [CrossRef]
62. Wang, J.; Wang, G.; Wu, C.; Li, J.; Cao, C.; Li, J.; Xie, Y.; Ge, S.; Chen, J.; Zeng, L.; et al. Enhanced aqueous-phase formation of secondary organic aerosols due to the regional biomass burning over North China Plain. *Environ. Pollut.* **2020**, *256*, 113401. [CrossRef] [PubMed]
63. Wu, Z.; Zhao, H.; Hao, J.; Wu, G. Climatological Characteristics and Aerosol Loading Trends from 2001 to 2020 Based on MODIS MAIAC Data for Tianjin, North China Plain. *Sustainability* **2022**, *14*, 1072. [CrossRef]
64. Du, H.; Li, J.; Wang, Z.; Dao, X.; Guo, S.; Wang, L.; Ma, S.; Wu, J.; Yang, W.; Chen, X.; et al. Effects of Regional Transport on Haze in the North China Plain: Transport of Precursors or Secondary Inorganic Aerosols. *Geophys. Res. Lett.* **2020**, *47*, e2020GL087461. [CrossRef]
65. Liu, X.; Chen, Q.; Che, H.; Zhang, R.; Gui, K.; Zhang, H.; Zhao, T. Spatial distribution and temporal variation of aerosol optical depth in the Sichuan basin, China, the recent ten years. *Atmos. Environ.* **2016**, *147*, 434–445. [CrossRef]
66. Srivastava, R. Trends in aerosol optical properties over South Asia. *Int. J. Climatol.* **2017**, *37*, 371–380. [CrossRef]